17th Australasian Fluid Mechanics Conference
Auckland, New Zealand
5-9 December 2010

Steady Inflow Through a Model Aneurysm: Global and Transient Stability

G. J. Sheard and H. M. Blackburn

Department of Mechanical and Aerospace Engineering, Monash University, Victoria 3800, Australia

Abstract

The stability of flow through a model aneurysm is numerically computed using a global linear stability analysis and a direct transient growth analysis. The geometry features a sinusoidal bulge in an otherwise uniform circular pipe, with dimensions representative of a human abdominal aortic aneurysm. With a time-independent inflow, the flow is weakly unstable to quasi-periodic global eigenmodes of azimuthal wavenumbers 4 and 5 at a Reynolds number (based on area-averaged velocity and pipe diameter) $Re \approx 3900$. These eigenmodes are concentrated in the outer part of the bulge, in the vicinity of its downstream end. A transient growth analysis reveals that the flow is sensitive to transient disturbances beyond $Re = 33$, well below the time-averaged Reynolds numbers of blood flow in the human abdominal aorta.

Introduction

Pipe flows arise in myriad engineering and biological systems, and hence have been a constant focus of fluid mechanics research for more than a century. The stability of flow in pipes is of particular interest, as transition from laminar to turbulent flow leads to a significant change in the flow dynamics. Moreover, particularly with application to biological flows in the cardiovascular system, changes in the symmetry of flows through the development of instabilities can markedly alter near-wall velocity profiles, and hence wall shear stress. This can exacerbate cardiovascular diseases such as atherosclerosis [10] and aneurysm [15].

Cardiovascular disease is a major health concern. For instance, 18% of Australians suffer a long-term cardiovascular condition, and 11% of the National health expenditure is incurred due to this disease [1]. In recent years, studies have elucidated the stability of flow through constricted pipe geometries designed to model stenosis (e.g. see [5, 7] and references therein). However, research into aneurysm disease, which manifests through a localized dilation of an artery due to degradation of wall tissue integrity, has primarily focused on patient-specific simulation [9]. Exceptions include recent laboratory experiments [11] and numerical simulations [13] in axisymmetric aneurysm models at physiologically relevant Reynolds numbers. These determined the wall shear stress distribution across, and flow structure within, an aneurysm bulge. The laboratory experiments employed particle image velocimetry in a plane bisecting the bulge, and inspection of their visualizations reveals slight asymmetry across the bulge centreline. This hints that these flows may be susceptible to non-axisymmetric instabilities.

The aim of this study is to investigate both the asymptotic stability and potential for transient growth within the flow through an axisymmetric model aneurysm, shown in figure 1. Fully developed Poiseuille flow with an area-averaged velocity U, flows from left to right. The fluid is Newtonian with kinematic viscosity ν, and a Reynolds number is defined based on the un-dilated pipe diameter D as

$$Re = \frac{UD}{\nu}.$$

Aneurysm flows in humans can experience time-averaged and peak Reynolds numbers of $Re \approx 300$ and $Re \approx 2000$ to 3000, respectively [11, 9]. These values guide the Reynolds number range of $Re \leq 8000$ investigated in the present study.

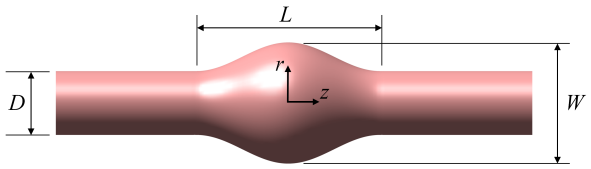

Figure 1: The geometry under investigation in this paper: the length (L) and width (W) of the bulge and the un-dilated pipe diameter D are shown. The bulge profile is sinusoidal.

Reproducing the aneurysm geometry considered in [13], the pipe features a smooth bulge with a sinusoidal profile. The bulge length and maximum diameter are $2.9D$ and $1.9D$, consistent with *Model 3* in [11]). Despite linear stability of Hagen–Poiseuille flow, one expects turbulence to appear in the straight downstream pipe at higher Reynolds number.

Methodology

The flows described in this study are computed by solving the incompressible Navier–Stokes equations formulated in cylindrical coordinates. A nodal spectral-element method is used for spatial discretization, and time integration is performed using backwards differencing [8]. The code follows a formulation in cylindrical coordinates [4], and solves the momentum and mass conservation equations,

$$\begin{aligned} \partial_t \mathbf{u} &= -(\mathbf{u}\cdot\nabla)\,\mathbf{u} - \nabla p + \nu\nabla^2\mathbf{u}, \\ \nabla\cdot\mathbf{u} &= 0, \end{aligned}$$

where ∂_t denotes a partial derivative with respect to time t, $\mathbf{u}$ is the velocity vector, and p is the kinematic static pressure.

Linear stability analysis

Asymptotic stability of the axisymmetric base flows ($\mathbf{U}$, P) to three-dimensional perturbations ($\mathbf{u}'$, p') is determined using a linear stability analysis. Linearizing about the base flow yields the linearized Navier–Stokes equations describing the evolution of the perturbation field

$$\begin{aligned} \partial_t \mathbf{u}' &= -(\mathbf{U}\cdot\nabla)\,\mathbf{u}' - (\mathbf{u}'\cdot\nabla)\,\mathbf{U} - \nabla p' + \nu\nabla^2\mathbf{u}', \\ \nabla\cdot\mathbf{u}' &= 0. \end{aligned} \tag{1}$$

A Fourier decomposition discretizes the three-dimensional perturbation field in the azimuthal direction, and linearity decouples individual Fourier modes. This permits the stability of individual azimuthal wavenumbers (m) to be computed separately on the same axisymmetric domain as used for the base flow computations.

An operator $\mathscr{A}(T)$ is defined describing the action of integrating equation (1) over a time interval T from an initial perturbation $\mathbf{u}'(t=0)$ such that $\mathbf{u}'(T) = \mathscr{A}(T)\mathbf{u}'(0)$. Solutions of equation (1) can be decomposed into solutions of the form

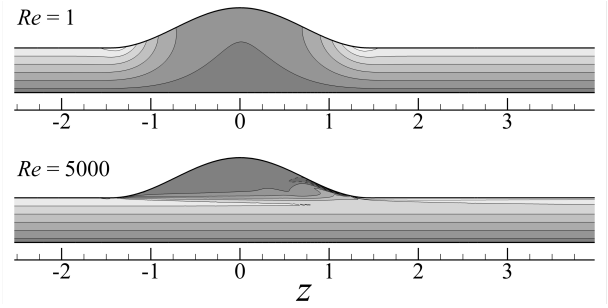

Figure 2: Contour plots showing the azimuthal component of vorticity in the vicinity of the bulge from axisymmetric simulations at Reynolds numbers $Re = 1$ and $Re = 5000$. 12 equispaced vorticity contour levels are plotted between $\omega_\theta \pm 8U/D$, with dark and light shading showing negative and positive vorticity, respectively.

$\tilde{\mathbf{u}}(\mathbf{x})\exp(\sigma t)$, where σ is the complex growth rate of individual eigenfunctions $\tilde{\mathbf{u}}(\mathbf{x})$. Stability is dictated by leading eigenmodes of the eigenproblem

$$\mathscr{A}(T)\tilde{\mathbf{u}}_j = \mu_j \tilde{\mathbf{u}}_j,$$

where $\tilde{\mathbf{u}}_j$ are eigenvectors corresponding to eigenvalues μ_j. The eigenvalue relates to the growth rate of an eigenmode through $\mu = \exp(\sigma T)$, and instability is predicted when $|\mu| > 1$. The linear stability analysis capabilities of the code have been successfully employed in recent studies [14, 3].

Transient growth analysis

In contrast to the asymptotic behaviour of linear perturbations predicted by linear stability analysis, evolution over short times may result in significant amplification due to the non-normality of eigenmodes of $\mathscr{A}$ [12]. Transient growth analysis seeks to determine the maximum possible amplification in energy (G) for a perturbation evolved over a time interval τ, and the corresponding initial field leading to this optimal growth ($\mathbf{v}$). These have been shown to be equivalent to the square of the leading singular value (λ) and the leading right singular vector of $\mathscr{A}$, respectively.

The square of the principal singular value and right singular vector of $\mathscr{A}$ are equivalent to the leading eigenvalue and eigenvector of $\mathscr{A}^*\mathscr{A}$, where $\mathscr{A}^*$ is the conjugate transpose (adjoint) of $\mathscr{A}$. This relationship has been used [2] to develop a method for predicting transient growth of a flow without explicitly constructing $\mathscr{A}$ or $\mathscr{A}^*$. They derived the adjoint linearized Navier–Stokes equations

$$\begin{aligned} -\partial_t \mathbf{u}^* &= (\mathbf{U}\cdot\nabla)\mathbf{u}^* - (\nabla\mathbf{U})^{\mathrm{T}}\cdot\mathbf{u}^* - \nabla p^* + \nu\nabla^2\mathbf{u}^*, \\ \nabla\cdot\mathbf{u}^* &= 0, \end{aligned} \tag{2}$$

such that the evolution of a perturbation backwards in time describes the action of $\mathscr{A}^*$ on a perturbation. Therefore, the action of $\mathscr{A}^*\mathscr{A}$ may be achieved by first integrating a perturbation forward in time over τ using equation (1), and subsequently integrating the result backwards in time using equation (2). Transient growth is then governed by the leading eigenmodes of

$$\mathscr{A}^*\mathscr{A}(\tau)\mathbf{v}_j = \lambda_j \mathbf{v}_j.$$

Discretization and grid independence

The mesh used in this study discretized the meridional half-plane of the geometry, and comprised 1603 elements. In order to accommodate the perturbation fields arising during transient growth analysis, the domain extended upstream and downstream of the bulge for the relatively large distances of $19D$ and $44D$, respectively. To resolve flow features, elements were concentrated within and downstream of the bulge.

To determine grid independence, the convergence of transient growth eigenvalues with increasing element polynomial degree (N_p) was computed. Reynolds numbers $Re = 300$ and 5000 were considered, corresponding respectively to approximately the time-averaged Reynolds number for flow through a human abdominal aorta, and a value exceeding the peak Reynolds number in these vessels. At $Re = 5000$, simulations with $N_p \leq 5$ failed to achieve a time-invariant state. At $N_p = 6$, G converged to within 6 and 3 significant figures for $Re = 300$ and 5000, respectively. A resolution of $N_p = 6$ is hence used hereafter.

Results

Reynolds number dependence of axisymmetric flow

Plots showing the azimuthal component of base flow vorticity at several Reynolds numbers are shown in figure 2. The flow quickly adopts the uniform vorticity field associated with fully developed Poiseuille flow outside of the bulge. Upstream, the flow only deviates visibly from Poiseuille flow as the bulge begins to expand, while the recovery distance downstream of the bulge is seen to increase with Reynolds number, though even at $Re = 5000$, the flow appears to recover within just a few diameters of the bulge. Secondly, the vorticity at the wall (which is closely related to wall shear stress [13]) is lower within the bulge than in the un-dilated tube. This difference becomes more pronounced at higher Reynolds numbers.

As Reynolds number increases, the flow entering the bulge displays a greater tendency to separate near the entrance, before proceeding through the core of the bulge and into the downstream pipe. Another notable feature of these flows is the vorticity field in the vicinity of the downstream end of the bulge and the periphery of the core region. At higher Reynolds numbers a steady-state waviness develops in the vorticity and flow fields. Ultimately this region of the flow is observed to become temporally unstable as the Reynolds number is increased beyond $Re \approx 7 \times 10^3$.

Asymptotic flow stability

As reviewed in [12], it is well-known that fully developed Poiseuille flow in a straight circular pipe is asymptotically stable to all linear disturbances, though in practice turbulence develops at higher Reynolds numbers. Given that in this geometry the uniform Poiseuille flow is disrupted by the presence of the bulge, it is possible that these flows may be unstable to global linear instability modes. A detailed linear stability analysis was conducted over a wide range of Reynolds numbers and azimuthal wavenumbers to determine the asymptotic stability of this system.

With increasing Reynolds number the flow first becomes unstable via a quasi-periodic mode with wavenumber $m = 4$ at $Re = 3910$, closely followed by another quasi-periodic mode with $m = 5$ at $Re = 4040$. Despite the steady-state axisymmetric flow becoming unsteady beyond $Re \approx 7 \times 10^3$, the zero-wavenumber mode remains highly stable throughout the range of Reynolds numbers investigated here, implying that the onset of unsteady flow observed in axisymmetric simulations is not a result of a global instability.

Contour plots of the first two eigenmodes to become unstable are shown in figure 3 at $Re = 4000$. The perturbation fields of

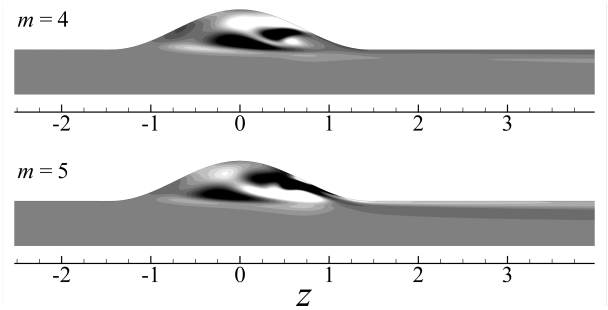

Figure 3: The leading eigenvector fields from linear stability analysis of azimuthal wavenumbers $m = 4$ and 5 at $Re = 4000$. Equi-spaced contours of the azimuthal component of vorticity is shown, with dark and light shading showing negative and positive vorticity, respectively. The predicted perturbation fields are concentrated within the bulge, surrounding the bulge core.

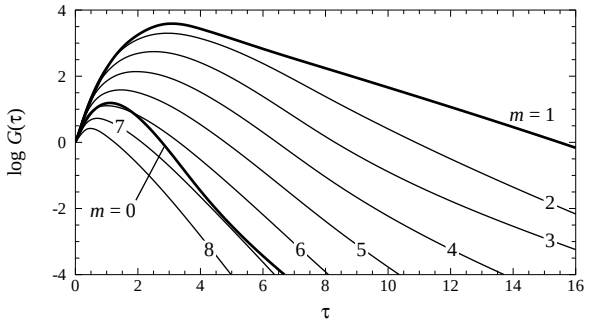

Figure 4: Logarithm of G plotted against τ at $Re = 300$. Wavenumbers $m = 0$ to 8 are shown as labelled.

the leading instability modes are concentrated within the region of the bulge outside of the core flow. The absence of perturbation field structures outside of the bulge reflects the absolutely stable Poiseuille flow in those regions.

Transient growth: Wavenumber variation

It has been shown (e.g. see [12, 5]) that flows exhibiting limited asymptotic instability may still exhibit substantial growth over short timescales. For stenotic flows transient growth can invoke bypass transition, where transient shear layer instability supersedes the predicted global instability transition path.

Ultimately, growth of azimuthal disturbances with higher wavenumbers is suppressed by viscosity. Figure 4 plots transient growth behaviour at $Re = 300$ across several azimuthal wavenumbers. Note that the greatest growth is found for the first azimuthal wavenumber. This was consistent across a range of Reynolds numbers, and is emerging as a general observation in confined flow through axisymmetric geometries. Examples include Hagen–Poiseuille flow [12], stenotic pipe flow [5] and flow through a suddenly expanded pipe [6].

The peak energy growth predicted at $Re = 300$ and $m = 1$ occurs at $\tau = 3.082$ with an amplification of $G_{\max} = 36.21$. By comparison, this amplification is much smaller than in stenotic pipe flow [5], where $G_{\max} \approx 5.6 \times 10^4$ at $\tau_{\max} \approx 3.3$.

Transient growth: Reynolds number variation

Transient growth for azimuthal disturbances with $m = 1$ at several Reynolds numbers are plotted in figure 5. Energy growth is found to increase in amplification and temporal envelope

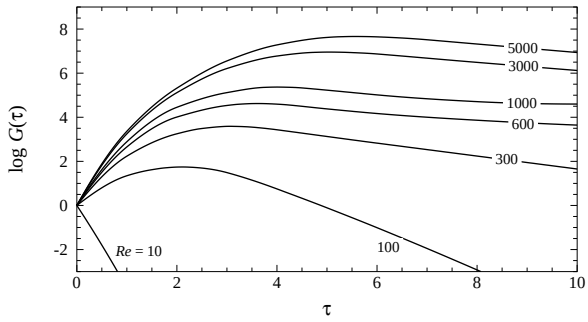

Figure 5: Logarithm of G plotted against τ for perturbations with $m = 1$ at Reynolds numbers as labeled. Maximum growth increases with both Re and τ.

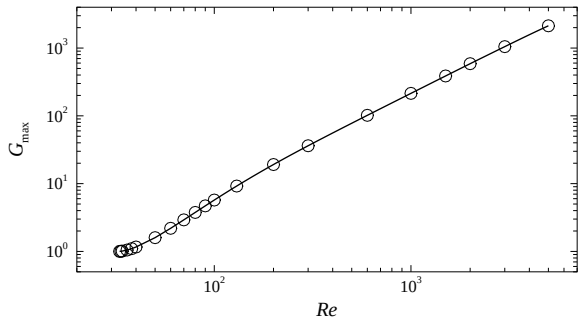

Figure 6: $G_{\max}$ plotted against Re for maximum growth for perturbations with azimuthal wavenumber $m = 1$, on a logarithmic scale.

with increasing Reynolds number. Further computations revealed that the critical Reynolds number for energy growth (i.e. $G(\tau) > 1$) is $Re_{\text{crit}} = 32.9$, more than two orders of magnitude below the predicted transition Reynolds number for global instability ($Re = 3910$).

The variation of peak growth with Reynolds number is plotted in figure 6. Two linear regions are identified (over $50 \lesssim Re \lesssim 150$ and $Re \gtrsim 200$), implying power-law dependencies of $G_{\max} \propto Re^{9/5}$ and $G_{\max} \propto Re^{7/5}$, respectively. These different growth trends in these regions may relate to changes in the underlying axisymmetric base flows. At Reynolds numbers below the first of these regions, the flow remains attached to the bulge wall. Over $50 \lesssim Re \lesssim 150$, the flow separates within the bulge, and a progressively larger recirculation bubble appears. At higher Reynolds numbers, the bulge recirculation enlargement ceases as it occupies the entirety of the bulge outside the core region.

Snapshot sequences of disturbance energy in the flow are shown in figure 7 showing initially the amplification of the disturbances to their respective peak times, before subsequently decaying as the disturbance advects downstream of the bulge. The disturbance structures are observed to shear and slant backwards as they move down the pipe, due to the faster flow along the axis of the pipe than towards the wall.

Conclusions

Computations have revealed that the steady flow through an axisymmetric aneurysm model with bulge length and width 2.9 and 1.9 times the pipe diameter, respectively, are unstable to weak transient disturbances with azimuthal wavenumber $m = 1$ beyond $Re \approx 33$. Eventually, the flow becomes unsta-

(*a*)

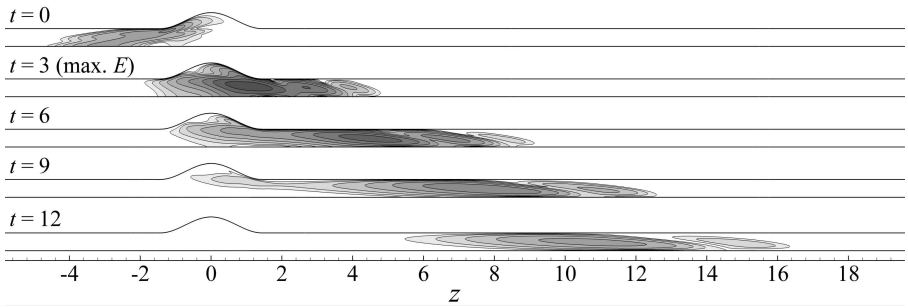

(*b*)

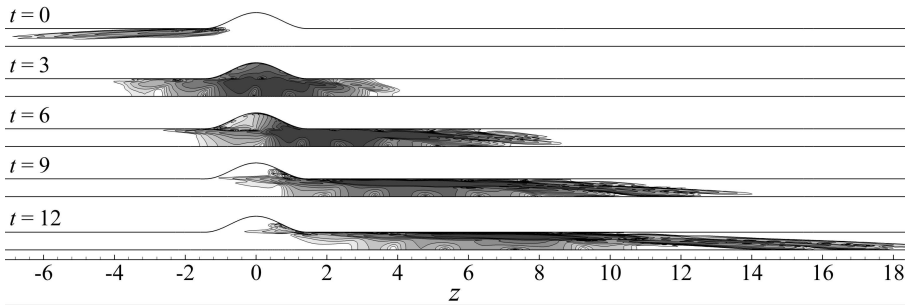

Figure 7: Time evolution of the predicted initial disturbance of azimuthal wavenumber $m = 1$ for optimal growth at (a) $Re = 300$ with $\tau = 3$, and (b) $Re = 5000$ at $\tau = 5.5$, integrated using the linearized Navier–Stokes equations. The logarithm of kinetic energy is plotted with unit spacing between contours, and darker shading corresponds to higher energy levels. Flow is left to right, and the meridional half-plane of the geometry is shown.

ble to quasi-periodic global instability modes with azimuthal wavenumbers $m = 4$ and 5 at $Re \approx 4000$. Three-dimensional direct numerical simulation will be required to determine if the predicted optimal disturbances could invoke bypass transition in aneurysm flows.

Acknowledgements

Computations were performed on the NCI National Facility in Canberra, Australia, which is supported by the Australian Commonwealth Government. G.J.S. received financial support from a Faculty of Engineering Small Grant, Monash University.

References

[1] Australian Bureau of Statistics, Canberra, Australia, *4821.0.55.001 - Cardiovascular Disease in Australia: A Snapshot, 2004-05*, 2006.

[2] Barkley, D., Blackburn, H. M. and Sherwin, S. J., Direct optimal growth analysis for timesteppers, *Intnl J. Num. Meth. Fluids*, **57**, 2008, 1435–1458.

[3] Blackburn, H. M. and Sheard, G. J., On quasi-periodic and subharmonic Floquet wake instabilities, *Phys. Fluids*, **22**, 2010, 031701.

[4] Blackburn, H. M. and Sherwin, S. J., Formulation of a Galerkin spectral element-Fourier method for three-dimensional incompressible flow in cylindrical geometries, *J. Comput. Phys.*, **197**, 2004, 759–778.

[5] Blackburn, H. M., Sherwin, S. J. and Barkley, D., Convective instability and transient growth in steady and pulsatile stenotic flows, *J. Fluid Mech.*, **607**, 2008, 267–277.

[6] Cantwell, C. D., Barkley, D. and Blackburn, H. M., Transient growth analysis of flow through a sudden expansion in a circular pipe, *Phys. Fluids*, **22**, 2010, 034101.

[7] Griffith, M. D., Thompson, M. C., Leweke, T. and Hourigan, K., Convective instability in steady stenotic flow: Optimal transient growth and experimental observation, *J. Fluid Mech.*, **655**, 2010, 504–514.

[8] Karniadakis, G. E., Israeli, M. and Orszag, S. A., High-order splitting methods for the incompressible Navier-Stokes equations, *J. Comput. Phys.*, **97**, 1991, 414–443.

[9] Lasheras, J. C., The biomechanics of arterial aneurysms, *Ann. Rev. Fluid Mech.*, **39**, 2007, 293–319.

[10] Malek, A. M., Alper, S. L. and Izumo, S., Hemodynamic shear stress and its role in atherosclerosis, *J. Amer. Med. Assoc.*, **282**, 1999, 2035–2042.

[11] Salsac, A.-V., Sparks, S. R., Chomaz, J.-M. and Lasheras, J. C., Evolution of the wall shear stresses during the progressive enlargement of symmetric abdominal aortic aneurysm, *J. Fluid Mech.*, **560**, 2006, 19–51.

[12] Schmid, P. J. and Henningson, D. S., Optimal energy density growth in Hagen–Poiseuille flow, *J. Fluid Mech.*, **277**, 1994, 197–225.

[13] Sheard, G. J., Flow dynamics and wall shear stress variation in a fusiform aneurysm, *J. Eng. Math.*, **64**, 2009, 379–390.

[14] Sheard, G. J., Fitzgerald, M. J. and Ryan, K., Cylinders with square cross section: Wake instabilities with incidence angle variation, *J. Fluid Mech.*, **630**, 2009, 43–69.

[15] Shojima, M., Oshima, M., Takagi, K., Torii, R., Hayakawa, M., Katada, K., Morita, A. and Kirino, T., Magnitude and role of wall shear stress on cerebral aneurysm - Computational fluid dynamic study of 20 middle cerebral artery aneurysms, *Stroke*, **35**, 2004, 2500–2505.